Korean J. Chem. Eng., 39(7), 1839-1849 (2022)
DOI: 10.1007/s11814-021-1015-x

pISSN: 0256-1115
eISSN: 1975-7220

Removal of Cr(VI) from solution using UiO-66-NH_2 prepared in a green way

Xiaoting Zhang*, Shusheng Zhang, Gangfeng Ouyang**, and Runping Han*,†**

*College of Chemistry, Green Catalysis Center, Zhengzhou University, No 100 of Kexue Road, Zhengzhou, 450001, P. R. China
**Center for Modern Analysis and Gene Sequencing, Zhengzhou University, No 100 of Kexue Road, Zhengzhou, 450001, P. R. China
(*Received 27 September 2021 • Revised 12 November 2021 • Accepted 14 November 2021*)

Abstract−A zirconium-based metal organic framework (UiO-66-NH_2) was prepared using a greener approach for the removal of hexavalent chromium (Cr(VI)) from solution. The characterization of UiO-66-NH_2 was performed using several methods, and the influence of the solution pH, adsorbent dosage, salt, adsorption time, Cr(VI) concentration and adsorption temperature on adsorption quantity was performed in batch mode. UiO-66-NH_2 can efficiently remove Cr(VI) through the synergistic effect of adsorption and reduction. At pH solution of 1.1 and solid-to-liquid ratio of 2 $g \cdot L^{-1}$, the removal rate of 100 $mg \cdot L^{-1}$ Cr(VI) increased to 95.2%. The maximum adsorption capacity of UiO-66-NH_2 from Langmuir model was 252 $mg \cdot g^{-1}$. The adsorption equilibrium process can be well described by Langmuir, Koble-Corrigan and Temkin models, while the kinetic process can be predicted by pseudo-second-order and Elovich model. UiO-66-NH_2 showed a good adsorption capacity in a wide range of pH (pH=1.1-10) and also had better regeneration performance after five cycles using 0.01 $mol \cdot L^{-1}$ NaOH; consequently, it can be a promising adsorbent for the removal of Cr(VI) from solution.

Keywords: Adsorption, UiO-66-NH_2, Hexavalent Chromium, Desorption

INTRODUCTION

Hexavalent chromium (Cr(VI)), as one of the most toxic pollutants in water bodies, has created great concern around the world. The pollution of Cr(VI) is mainly through the discharge of industrial wastewater, such from metal polishing, electroplating, textile dyeing, alloying, chromium salt and leather processing industries [1,2]. Cr(VI) (mainly in the form of CrO_4^{2-} and $Cr_2O_4^{2-}$) is characterized by high water solubility, non-degradability, and bioaccumulation, and is highly toxic; consequently, it can easily cause cancer when entering the human body [3,4]. According to the World Health Organization, the contaminant level of Cr(VI) in drinking water should not exceed 0.05 $mg \cdot L^{-1}$ [5,6]. Therefore, it is necessary to control the discharge of Cr(VI) from the sources as well as reduce the chromium content in the polluted water bodies.

At present, various treatment methods, such as adsorption, chemical precipitation, ion exchange, photocatalysis, reverse osmosis and electrodialysis, have been employed to remove chromium from water and wastewater [7,8]. Between these methods, adsorption is highly valued as it has several advantages, including simple technology, high efficiency, low cost with no secondary pollution produced [9]. Recently, a number of adsorbents, including surface-modified magnetic nanoparticles [10], carbon-based materials [11,12] and natural polymer [13-16], have been widely used to remove chromium from solution. However, most of these adsorbents have some shortcomings, so it is still necessary to find an effective adsorbent to capture Cr(VI).

In water systems, chromium can exist in two valence states: (Cr(VI) and Cr(III)) [13-16]. For high toxicity of Cr(VI), excess chromium usually exists in the form of Cr(III) and is an essential nutrient element for mammals [17]. However, it is costly and difficult to directly reduce Cr(VI) to Cr(III). Therefore, the adsorbent with catalytic degradation activity can be considered to realize the synergistic performance of the adsorption and reduction of Cr(VI). This not only saves cost, but also effectively reduces the pollution of Cr(VI) in water bodies.

Application of the metal-organic frameworks (MOFs) in water and wastewater remediation cannot be underestimated as these materials are observed to possess higher surface area, large porosity, intrinsic function and multifunctional structure [18-20]. All these surface features play paramount roles in the adsorption process. However, some MOF materials have certain limitations in water treatment due to their poor water stability. Compared with other MOFs, Zr-MOF has attracted wide attention for its good water stability [21,22]. However, most Zr-MOF synthesis processes are accompanied with the use of organic compound reagents (such as N, N-Dimethylformamide) which have higher level of toxicity [23]. At the same time, there is an increasing of the processing cost of removing secondary pollutants during the synthesis process. This point is not consistent with the concept of green chemistry; therefore, it is essential to find an economical, environmentally friendly and efficient method for the preparation of Zr-MOF.

In our previous study, formic acid and ethanol were selected as solvents, and zirconium chloride and 2-aminoterephthalic acid were used as ligand acceptors and donors to synthesize UiO-66-NH_2 under mild conditions [24]. This UiO-66-NH_2 adsorbent had good adsorption property towards phosphate. Therefore, in this study, UiO-66-NH_2 was utilized to enhance the synergistic effect of adsorption and reduction of Cr(VI) from aqueous solution. This adsorbent greatly minimized the direct cost of reducing the highly toxic

†To whom correspondence should be addressed.
E-mail: rphan67@zzu.edu.cn

Cr(VI) to the low-toxic Cr(III), and at the same time decontaminated the Cr(VI) in the solution. The effects of solution pH, adsorbent dosage, equilibrium concentration, adsorption time and temperature on adsorption were explored by batch experiments. Finally, the regeneration performance of the spent UiO-66-NH_2 and the feasibility of using it in actual wastewater treatment were explored. The adsorption mechanism was speculated by resorting to various analytical methods.

MATERIALS AND METHODS

1. Main Reagents

Materials: Absolute ethanol (C_2H_5OH) was obtained from Tianjin Fuyu Fine Chemical Co., Ltd. (China); Formic acid (HCOOH) was purchased from Tianjin Yongda Chemical Reagent Co., Ltd. (China); Potassium dichromate ($K_2Cr_2O_7$) was obtained from Jiaozuo Xin'an Technology Co., Ltd. (China); Zirconium chloride ($ZrCl_4$) and 2-aminoterephthalic acid ($C_8H_7NO_4$) were purchased from Shanghai Aladdin Biochemical Technology Co., Ltd. (China).

2. Synthesis of UiO-66-NH_2

The synthesis process was similar to that of the previous study [24]. Briefly, 0.466 g zirconium chloride and 0.181 g 2-aminoterephthalic acid were added in the mixed solvent of 25 mL of 30% formic acid and 20 mL of C_2H_5OH. Then, it was transferred to a polytetrafluoroethylene reactor for 12 h at 110 °C in a vacuum drying oven after the mixed solution was completely dissolved by ultrasonic treatment. The product was cooled to room temperature and then washed with ethanol and deionized water several times in sequence, and vacuum-dried at 60 °C for 12 h. Lastly, the final product (marked as UiO-66-NH_2) was obtained with the yield 0.440 g.

3. Characterization

A variety of characterization methods were used to analyze the performance of UiO-66-NH_2. First, the functional groups and the morphology on the surface of UiO-66-NH_2 were analyzed by FTIR analysis (PE-1710FTIR, American PE Company) and scanning electron microscope (SEM, Su8020, China Tianmei Scientific Instruments Co., Ltd.), respectively. Specific surface area analyzer (BET, ASAP2420, American Mike Co., Ltd.) was utilized to analyze the specific surface area. The crystal structure of UiO-66-NH_2 was confirmed using X-ray diffraction (XRD, Miniflex 600). X-ray photoelectric spectroscopy (XPS, Escalab 250Xi, Thermo Fisher Scientific) was used to determine the action form of adsorption.

4. Adsorption Test

A certain amount of UiO-66-NH_2 was added into several 50 mL conical flasks containing 10 mL of a certain concentration of Cr(VI) solution (calculated as Cr(VI)), and the flasks were shaken for a certain period of time at a specific temperature in a water bath. Following adsorption, the UiO-66-NH_2 adsorbent was separated from the mixture by centrifugation, and the concentration of the supernatant (Cr(VI)) was measured at wavelength of 540 nm in diphenylcarbazide spectrophotometry. The effects of the system pH (pH=1.1-12), adsorbent dosage (4-20 mg), salinity (0-0.2 mol·L^{-1}), adsorption time (0-6 h), temperature (293-313 K) and initial concentration (25-400 mg·L^{-1}) on adsorption were explored by batch experiments.

The unit adsorption capacity and removal rate were calculated by Eq. (1) and (2), respectively.

$$q = \frac{V(C_0 - C)}{m} \quad (1)$$

$$p = \frac{C_0 - C}{C_0} \times 100\% \quad (2)$$

where q is the unit adsorption quantity (mg·g^{-1}), m represents the mass of UiO-66-NH_2 (g), V indicates the volume of Cr(VI) solution (L), p shows the removal efficiency, C_0 (mg·L^{-1}) and C (mg·L^{-1}) express the concentration of adsorbate before and after adsorption.

5. Regeneration Performance

A certain amount of UiO-66-NH_2 was introduced into a conical flask having 300 mg·L^{-1} Cr(VI) solution and the mixture was shaken for 6 h at 303 K and 120 rpm. The unit adsorption capacity (q_e) was calculated. Cr-loaded adsorbent was washed three times by deionized water and dried in an oven at 60 °C for 12 h. Then 10 mg of spent UiO-66-NH_2 was added in 50 mL Erlenmeyer flask containing 10 mL of different desorption liquids (0.01 mol·L^{-1} sodium hydroxide solution, 0.005 mol·L^{-1} sodium hydroxide solution, a mixed solution of 0.005 mol·L^{-1} sodium hydroxide solution and 50% ethanol as well as 75% ethanol). The flasks were then shaken at 30 °C for 6 h and the desorption rate d was determined. The desorbed material was washed three times with deionized water, and the above operation was repeated, then the regeneration rate r was calculated. The better desorption solution was chosen for multiple desorption regeneration.

The d and r are calculated by Eq. (3) and (4), respectively.

$$d = m_d / m_0 \times 100\% \quad (3)$$

$$r = q_r / q_m \times 100\% \quad (4)$$

where m_d represents the mass of Cr(VI) in solution after desorption, m_0 indicates the mass of Cr(VI) on UiO-66-NH_2 before desorption, q_m and q_r mean the unit adsorption amount for the first and next adsorption, respectively.

6. Removal of Cr(VI) from Simulated Wastewater

Taking the lake water of Zhengzhou University as the simulated water sample, the Cr(VI) content of the lake water was not detected with pH=6.8. The actual amount of 10 mg UiO-66-NH_2 was added to each conical flask containing 10 mL of Cr(VI) solution with different concentration (0, 20, 50, 100 mg·L^{-1}), and then the mixtures in the flasks were shaken at 303 K for 6 h.

RESULTS AND DISCUSSION

1. Characterization of Materials

1-1. FTIR Analysis

FTIR analysis of UiO-66-NH_2 before and after adsorption was performed to determine the changes and contribution of the functional groups of UiO-66-NH_2 toward uptake of Cr(VI), and the results are shown in Fig. 1(a). It was observed that UiO-66-NH_2 showed a large and broad absorption peak at 3,430 cm^{-1}, which is ascribed to the presence of -NH_2 and -OH [24,25]. The peaks at 1,580 and 1,400 cm^{-1} are attributed to vibration of the benzene ring [26]. The absorption peaks observed at 1,260 cm^{-1} and 1,370 cm^{-1}

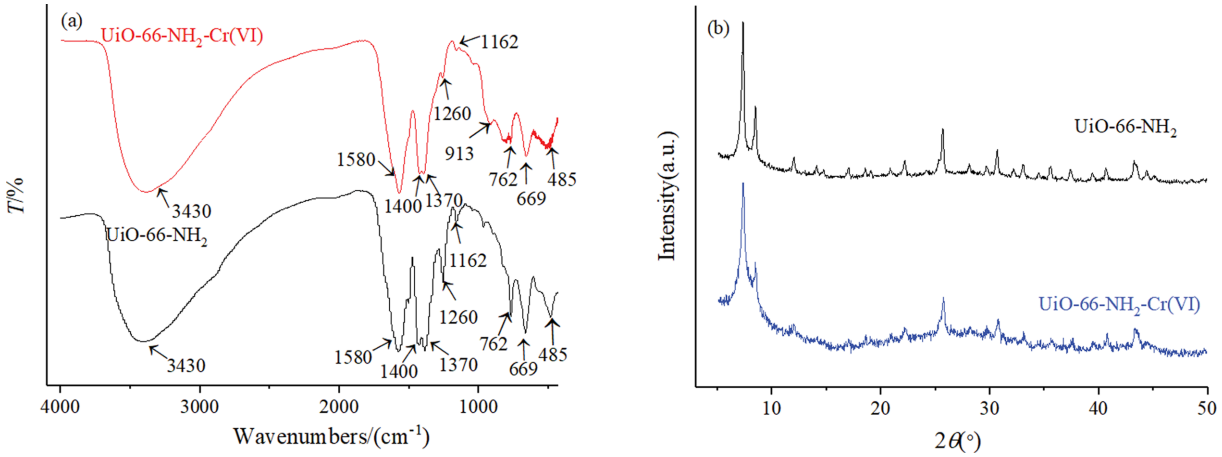

Fig. 1. (a) FTIR analysis before and after adsorption and (b) XRD of UiO-66-NH_2.

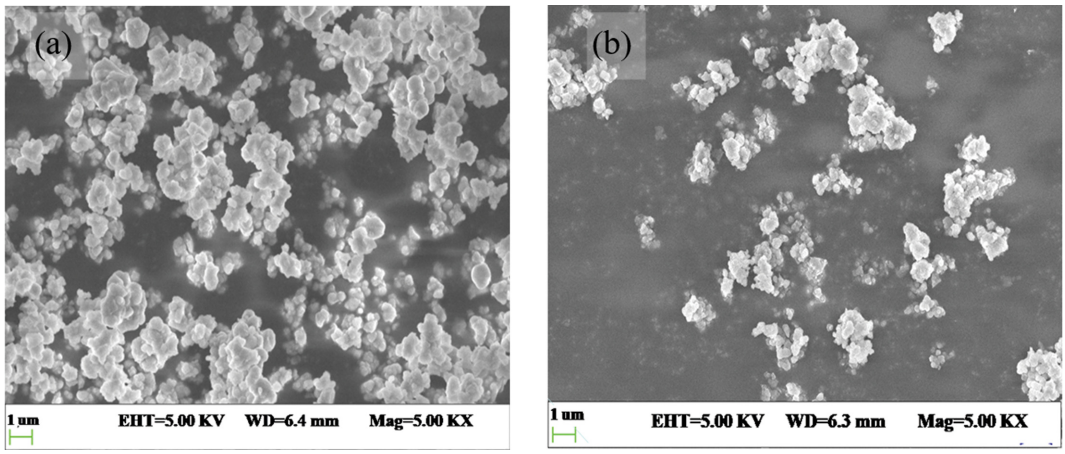

Fig. 2. SEM analysis of UiO-66-NH_2 (a) before and (b) after regeneration.

are the characteristic peaks of C-N bonded between aromatic carbon and nitrogen [18]. The absorption peak at 669 cm^{-1} can be attributed to vibration of Zr-O [27,28]. For the Cr-loaded UiO-66-NH_2, two peaks at 762 cm^{-1} and 485 cm^{-1} are broadened due to the existence of Cr-O (765 cm^{-1}) and Cr-O-Cr (604 cm^{-1}) bond, and a small peak at 913 cm^{-1} corresponds to the vibration of Cr=O bond [7,9], which confirms that Cr(VI) was successfully adsorbed by UiO-66-NH_2. Moreover, the peak intensity at 1,260 cm^{-1} on UiO-66-NH_2-Cr(VI) spectrum had significantly decreased. This revealed that -NH_2/-NH_3^+ on the surface of UiO-66-NH_2 may participate in the adsorption process, and it can also be understood that this process may involve electrostatic attraction [29]. In conclusion, FTIR analysis showed that Cr(VI) was successfully captured as well as the process was likely to proceed through the electrostatic attraction.

1-2. XRD Analysis

The XRD spectra of UiO-66-NH_2 before and after adsorption are presented in Fig. 1(b). The diffraction peaks of UiO-66-NH_2 obtained in this study are consistent with the ones reported in the previous studies [22,24], indicating that UiO-66-NH_2 was successfully prepared and has a high crystallinity. Moreover, the several diffraction peaks near 7.36°, 8.48°, 12.04°, 25.68° and 33.12° correspond to (111), (002), (022), (224), (137) crystal planes, respectively [24,30,31], which also demonstrates that the material had a crystalline structure. In addition, the main diffraction peaks of the material before and after adsorption did not change significantly, indicating that the crystal structure of the material remained unchanged during the adsorption process.

1-3. BET Analysis of UiO-66-NH_2

Fig. S1(a) shows the isotherm curve of N_2 adsorption. The isotherm curve of N_2 adsorption increased rapidly at $P/P_0<0.1$ (Fig. S1(a)) and this indicates the presence of micropores on the surface of UiO-66-NH_2. The isotherm exhibited a typical I-type structure with the presence of abundant micropores centered at 0.65 nm (Fig. S1(b)). Also, the BET analysis results showed that UiO-66-NH_2 had a surface area of 830.6 $m^2 \cdot g^{-1}$ (Langmuir surface area of 980.7 $m^2 \cdot g^{-1}$) and median pore width of 0.745 nm. These results indicate that the material had a larger specific surface area.

1-4. SEM Analysis

Moreover, as can be seen in Fig. 2(a), UiO-66-NH_2 material exhibited an agglomerated irregular three-dimensional morphology. This is consistent with the results obtained from XRD analysis, revealing that UiO-66-NH_2 had a crystalline structure. The three-dimensional structure of UiO-66-NH_2 is similar to a nano-scale

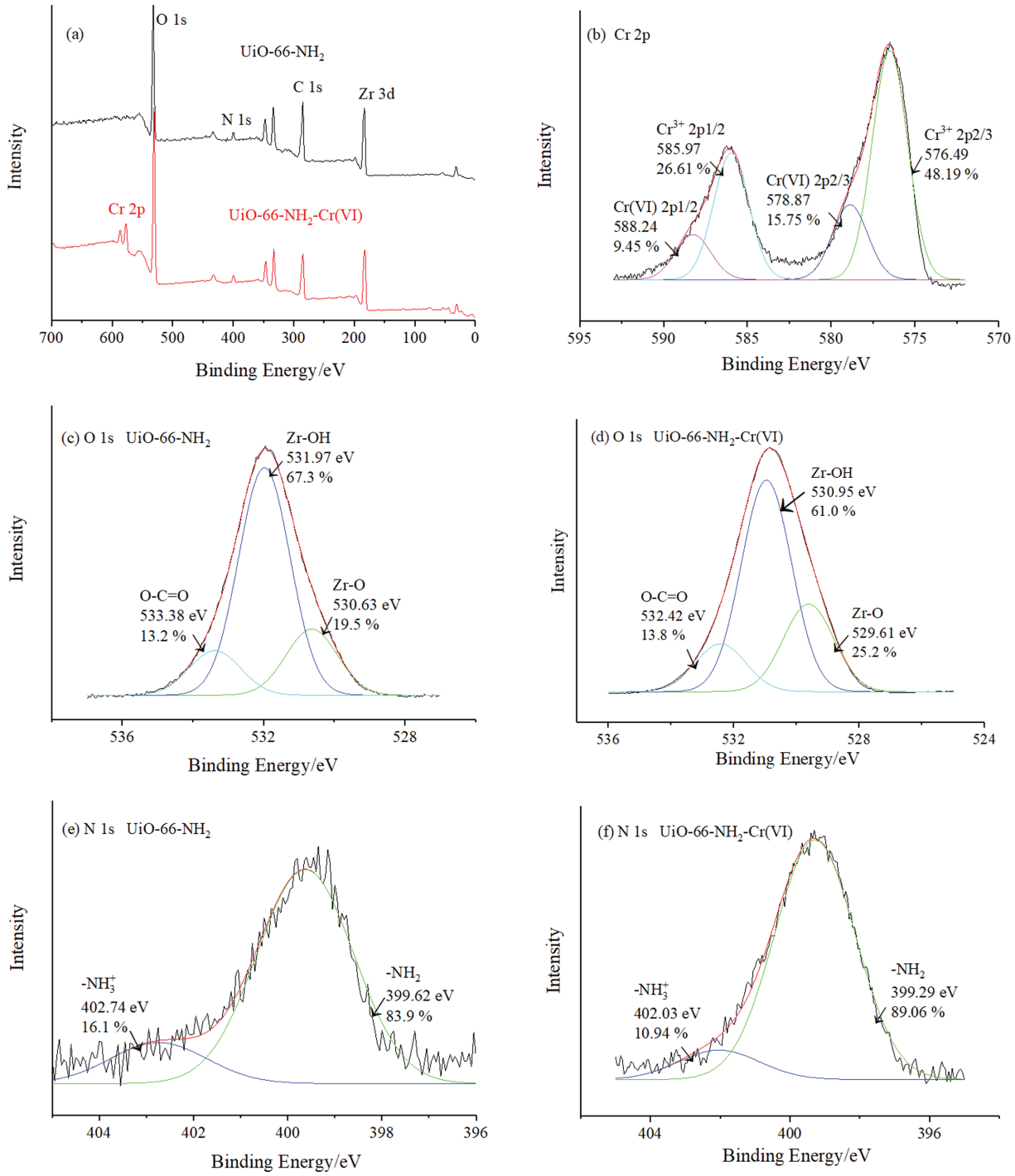

Fig. 3. (a) Wide scan of XPS for UiO-66-NH_2 before and after adsorption; High resolution spectra: (b) Cr 2p after adsorption, O 1s (c) before and (d) after adsorption, N 1s (e) before and (f) after adsorption.

sphere as it has higher specific surface area and irregular nano-scale particles. In addition, the surface morphology of UiO-66-NH_2 material was stable after five regeneration cycles (Fig. 2(b)). There was no significant difference of UiO-66-NH_2 morphology before and after adsorption of Cr(VI), indicating the stability of the material.

1-5. XPS Analysis

For understanding the adsorption mechanism, XPS analysis was carried out and the results are shown in Fig. 3. Compared with the total spectrum of UiO-66-NH_2 (Fig. 3(a)), a new energy spectrum peak appeared at 587 eV after adsorption of Cr(VI). This peak is attributed to Cr 2p.

After splitting the peak of Cr 2p, four peaks were obtained (Fig. 3(b)): two peaks at 576.49 and 585.97 eV are attributed to Cr(III), while those at 578.87 and 588.24 eV are ascribed to Cr(VI) [32]. The presence of Cr(III) indicates that some Cr(VI) was reduced to

Cr(III) on the surface of UiO-66-NH_2. This confirms the simultaneous occurrence of both adsorption and reduction of Cr(VI).

There was a significant difference between the split peaks of O 1s before and after adsorption. Before adsorption, three peaks of O 1s were formed at 530.63 (19.5%), 531.97 (67.3%) and 533.38 eV (13.2%) (Fig. 3(c)), which correspond to Zr-O, Zr-OH and O-C=O [33]. After adsorption, these three peaks shifted to lower binding energies, and located at 529.61 (25.24%), 530.95 (60.97%) and 532.42 eV (13.79%), respectively (Fig. 3(d)). The energy spectrum peak content of Zr-OH was significantly reduced. It denotes that Zr-OH was involved in the adsorption process; therefore, there may be complexation between Zr-OH and Cr(VI) in the form of Zr-O-Cr [31].

As for the split peaks of N 1s, two peaks were obtained at 399.62 and 402.74 eV of the N 1s before adsorption (Fig. 3(e)). These peaks are ascribed to -NH_2 (83.9%) and -NH_3^+ (16.1%) [24]. After adsorption, the two peaks slightly moved to lower binding energy (399.29, 402.03 eV) and the peak area changed (Fig. 3(f)). This confirmed that -NH_2/-NH_3^+ on the surface of UiO-66-NH_2 participated in the adsorption. It can be understood that there may be hydrogen bonding/electrostatic attraction between -NH_2/-NH_3^+ and Cr(VI).

In summary, XPS analysis showed that the adsorption process could be governed by electrostatic attraction, hydrogen bonding, complexation and reduction.

2. Adsorption Studies

2-1. Effect of pH

Generally, pH value provides a significant effect on the existence form of adsorbate and the surface property of adsorbent in the solution; as a result, it may influence the adsorption capacity of UiO-66-NH_2 on Cr(VI). So the effect of pH on adsorption process was performed and the results are shown in Fig. 4(a). It was observed that the adsorption capacity (q_e) of Cr(VI) decreased steadily as the pH increased from 1.1 to 12. This phenomenon can be explained by the involvement of electrostatic force. At solution pH 1-6, Cr(VI) existed mainly in negatively charged in the form of $HCrO_4^-$ and $Cr_2O_7^{2-}$ [10]. In addition, at this pH range, the surface charge of UiO-66-NH_2 became positive (as the isoelectric point of UiO-66-NH_2 was 6.2), and the degree of protonation enhanced with the increase of acidity. So the q_e of Cr(VI) increased from 45.6 to 82.8 mg·g^{-1} when the pH solution decreased from 6.1 to 1.1. At solution pH 6.2-10, the surface of UiO-66-NH_2 became negatively charged, and the degree of deprotonation increased with the increase of alkalinity. The electrostatic attraction became weak, but the adsorption performance of UiO-66-NH_2 on Cr(VI) had not significantly decreased (such that the values of q_e were not lower than 29.5 mg·g^{-1}). At this time, there should be complexation and hydrogen bonding between the material and Cr(VI) [34]. When the pH increased from 10 to 12, the adsorption capacity of UiO-66-NH_2 on Cr(VI) lessened rapidly from 29.5 to 2.85 mg·g^{-1}. This was because of the presence of large amount of OH^- ions that obstructed the progress of adsorption under higher alkaline conditions (pH=10-12) [35]. This phenomenon is relatable to the one reported by Lai et al. [36] on the application of UiO-66 based on N-doped carbon nanoparticles coated by PANI for removal of hexavalent chromium [36]. Nevertheless, UiO-66-NH_2 showed a wide pH range (1.1-10) for Cr(VI) adsorption. Considering that most of the Cr(VI)-containing wastewaters are acidic, therefore this study examined the adsorption performance of UiO-66-NH_2 on Cr(VI) under acidic conditions (using the solution pH 1.1).

2-2. Effect of Dosage of UiO-66-NH_2

To ensure the utilization of materials and the removal rate of adsorbate at the same time, the amount of adsorbent was investigated. The results are in Fig. S2(a). As shown in Fig. S2(a), as the mass of UiO-66-NH_2 increased from 2 to 20 mg, the unit adsorption capacity gradually decreased from 175 to 40 mg·g^{-1}, while the removal rate increased from 40% to 97%. This phenomenon can be explained by the increase of active sites in the system with the increase of Zr-MOF; therefore more Cr(VI) ions were captured from the solution. At fixed amount of Cr(VI) in the system, the removal efficiency of UiO-66-NH_2 showed an increasing trend; however, the corresponding q_e demonstrated a downward trend. Comprehensively considering the effective utilization of Zr-MOF and the removal efficiency of Cr(VI), the mass of Zr-MOF was selected as 10 mg in the follow-up study (the corresponding d>85% with the solid-to-liquid ratio as 1 g·L^{-1}).

2-3. Effect of Salinity

The coexisting ions often affect the adsorption quantity [37].

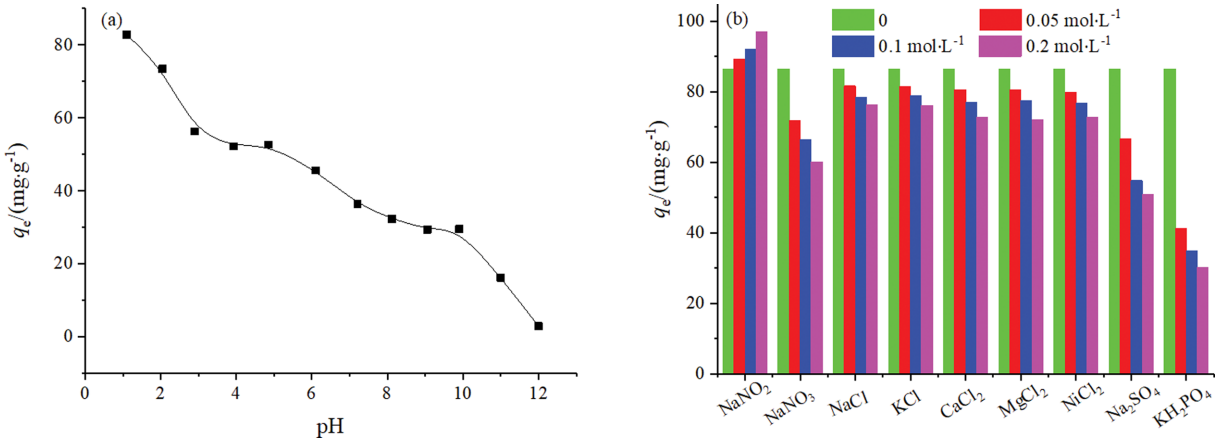

Fig. 4. Effect of pH (a) and salt (b) on adsorption.

The effect of salt was explored and the results are shown in Fig. 4(b). It was illustrated that the presence of these common coexisting ions (Na^+, K^+, Ca^{2+}, Mg^{2+}, Ni^{2+} and Cl^-) had basically no effect on the adsorption of Cr(VI). But some anions (NO_3^- and SO_4^{2-}) showed a weak negative effect on the adsorption of Cr(VI) with the adsorption capacity decreased by nearly a quarter as the salt concentration increased from 0 to 0.2 mol·L^{-1}. This showed that there may be electrostatic force and complexation during the adsorption process. However, the presence of NO_2^- showed a positive effect with the q_e raised from 86.5 to 97 mg·g^{-1} as the content of NO_2^- increased from 0 to 0.2 mol·L^{-1}, which may be because it promoted the conversion of Cr(VI) to Cr(III). In addition, the presence of phosphate showed a large negative effect, which may be due to the strong competitive adsorption between Cr(VI) and phosphate in the process. However, when the phosphate content was as high as 0.2 mol·L^{-1}, the adsorption capacity of UiO-66-NH_2 capturing Cr(VI) was still not less than 30 mg·g^{-1}. On the whole, the material had a certain salt tolerance.

2-4. Study on Adsorption Kinetics

To understand the rate of adsorption, the kinetics of adsorption was studied. The results are shown in Fig. 5(a)-(c). It was observed that the values of q_t toward Cr(VI) increased rapidly at first stage (0-1 h), in which 80% of the total adsorption quantity was absolutely attained. Then the adsorption gradually decreased with the increase of contact time from 1 to 5 h until the adsorption process reached equilibrium. Keeping the initial concentration of Cr(VI) constant, there were more active sites in the initial stage of adsorption, so the adsorption proceeded faster. However, the active sites on the surface of UiO-66-NH_2 were limited and decreased with the progress of adsorption until equilibrium was attained. In addition, at the same contact time, the values of q_t were higher with the increase of initial concentration. This was because more Cr(VI) ions participated in the adsorption process under the same conditions.

For understanding the adsorption behavior of Cr(VI) on UiO-66-NH_2, four models (shown in Table S1) were employed to fit the kinetic data. The fitting curves and corresponding parameters are shown in Fig. 5(a)-(c) and Table 1, respectively. The pseudo-first-order and pseudo-second-order models are suitable for describing the adsorption process led by physical adsorption and chemical adsorption, respectively [38,39]. It is seen from Table 1 that there is larger R^2 value ($R^2 \geq 0.890$) and smaller SSE value for the pseudo-second-order model. Moreover, the values of $q_{e(theo)}$ from this model are closer to values of $q_{e(exp)}$ from experiments and the fitting curves are also adjacent to the experimental curves. These suggested that the pseudo-second-order kinetic model is much better for describing the adsorption process of Cr(VI) onto UiO-66-NH_2, including chemical process.

Moreover, the Elovich and Double Constant models are often used to predict the heterogeneous diffusion process [38]. The large

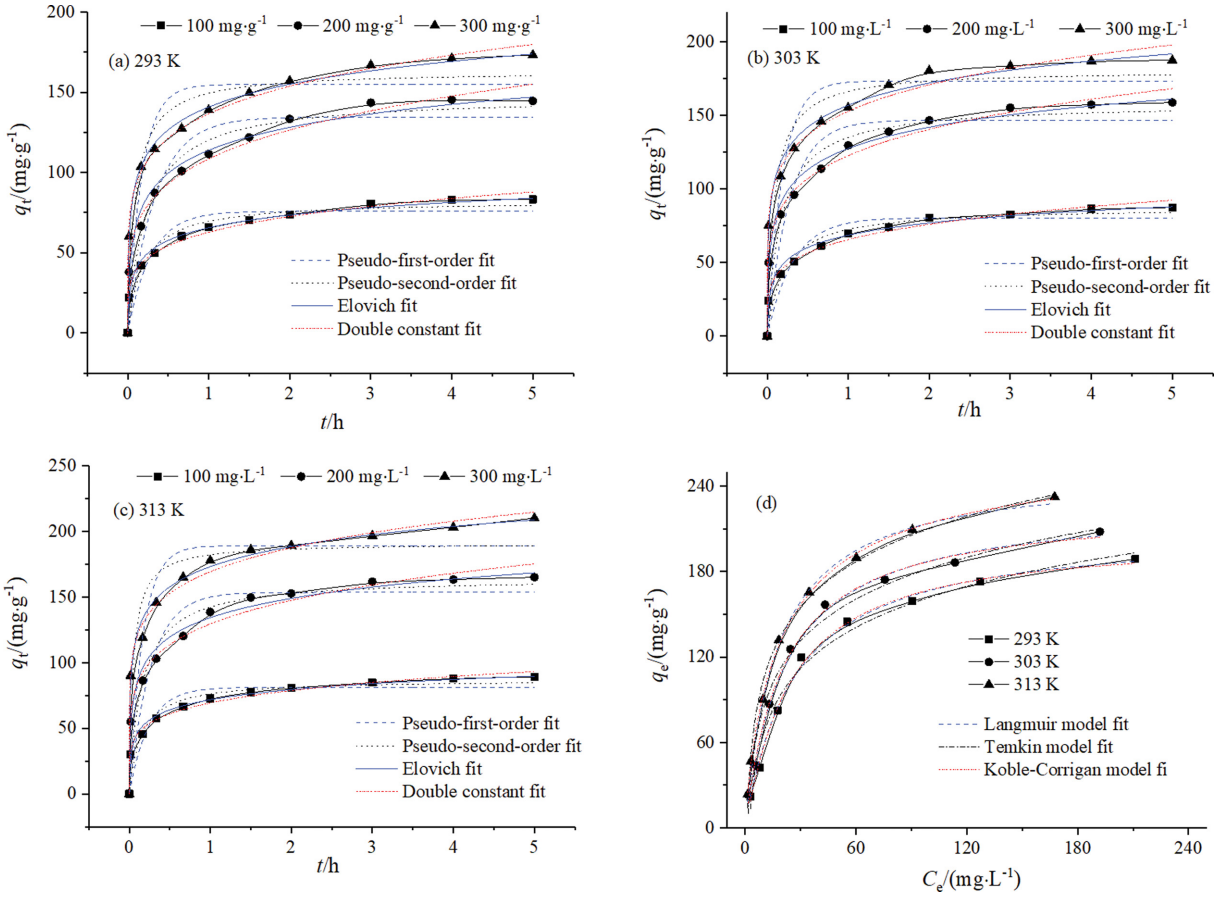

Fig. 5. Study on adsorption kinetics at various temperatures (a)-(c) and isotherms (d).

Table 1. Kinetic fitting parameters

Pseudo-first-order equation						
T/K	C_0/(mg·L^{-1})	$q_{e(exp)}$/(mg·g^{-1})	$q_{e(theo)}$/(mg·g^{-1})	k_1/(h^{-1})	R^2	SSE
293	100	83.2	75.8±4	3.53±0.84	0.896	674
	200	145	134±7	2.94±0.68	0.897	2,108
	300	173	155±8	5.71±1.81	0.841	4,077
303	100	87.4	80.3±3.9	3.12±0.73	0.897	741
	200	159	147±8	3.57±0.93	0.872	2,979
	300	187	173±10	5.27±1.66	0.827	5,295
313	100	89.2	81.2±4.2	4.17±1.12	0.869	923
	200	165	154±8	3.76±0.98	0.871	3,230
	300	210	189±11	5.99±2.03	0.810	6,752
Pseudo-second-order equation						
T/K	C_0/(mg·L^{-1})	$q_{e(exp)}$/(mg·g^{-1})	$q_{e(theo)}$/(mg·g^{-1})	k_2/(g·mg^{-1}·h^{-1})	R^2	SSE
293	100	83.2	82.4±3.5	0.0656±0.0186	0.949	332
	200	145	148±7	0.0297±0.0084	0.947	1,082
	300	173	163±8	0.0668±0.0265	0.915	2,166
303	100	87.4	87.5±4.0	0.0710±0.0159	0.945	394
	200	159	158±8	0.0371±0.0124	0.928	1,676
	300	187	181±9	0.0681±0.0275	0.899	3,094
313	100	89.2	86.9±4.2	0.0807±0.0281	0.924	534
	200	165	165±8	0.0389±0.0133	0.925	1,888
	300	210	191±9	0.109±0.052	0.890	3,888
Double constant equation						
T/K	C_0/(mg·L^{-1})	A		Ks	R^2	SSE
293	100	62.8±0.9		0.209±0.012	0.989	69.6
	200	108±2		0.222±0.015	0.986	286
	300	137±1		0.171±0.008	0.994	152
303	100	65.5±1.1		0.213±0.014	0.987	92.9
	200	123±2		0.196±0.012	0.988	280
	300	153±2		0.161±0.010	0.989	345
313	100	69.3±0.9		0.184±0.011	0.990	71.9
	200	130±2		0.188±0.014	0.984	404
	300	169±2		0.148±0.009	0.991	320
Elovich equation						
T/K	C_0/(mg·L^{-1})	A		B	R^2	SSE
293	100	65.6±0.7		11.4±0.4	0.994	38.1
	200	114±2		20.6±1.1	0.985	312
	300	141±1		20.5±0.6	0.997	74.5
303	100	68.5±1.0		12.0±0.6	0.988	89.0
	200	127±2		20.8±1.1	0.988	283
	300	157±2		21.6±1.1	0.990	301
313	100	71.7±0.8		11.1±0.5	0.991	63.6
	200	134±2		21.2±1.2	0.986	353
	300	173±2		22.1±1.1	0.991	314

values of R^2 ($R^2 \geq 0.984$) and small values of SSE (less than 404) are shown in Table 1 from both models and the fitted curve also shows a high degree of agreement. In short, both models well describe the adsorption process, including heterogeneous diffusion. Based on the above, heterogeneous chemical adsorption existed in the process of UiO-66-NH_2 capturing Cr(VI).

2-5. Study on Adsorption Isotherm

The adsorption isotherm was investigated in order to know the

Table 2. Isotherm fitting parameters

Langmuir					
T/K	K_L/(L·mg^{-1})	$q_{e(exp)}$/(mg·g^{-1})	$q_{m(theo)}$/(mg·g^{-1})	R^2	SSE
293	0.0381±0.0028	189	211±5	0.995	106
303	0.0458±0.0048	208	228±7	0.991	161
313	0.0571±0.0033	231	252±4	0.997	96.1
Koble-Corrigan					
T/K	A	B	n	R^2	SSE
293	6.74±1.62	0.0329±0.0071	1.07±0.09	0.995	95.3
303	10.9±2.5	0.0484±0.0097	1.00±0.09	0.994	137
313	20.7±1.7	0.0768±0.0052	0.851±0.037	0.999	39.3
Temkin					
T/K	A		B	R^2	SSE
293	−29.6±8.3		41.6±2.2	0.981	433
303	−13.1±9.2		42.4±2.6	0.975	693
313	−0.936±5.569		45.9±1.7	0.991	318

Table 3. Related thermodynamic parameters

E_a/(kJ·mol^{-1})	ΔH^0/(kJ·mol^{-1})	ΔS^0/(J·mol^{-1}·K^{-1})	ΔG^0/(kJ·mol^{-1})		
			293 K	303 K	313 K
8.21	29.0	0.117	−5.04	−6.55	−7.37

effect of adsorption temperature and equilibrium concentration on adsorption. The results are in Fig. 5(d). It was clearly observed that the values of q_e increased rapidly at first and then slowly but did not reach a platform with the increase of the equilibrium concentration of Cr(VI). This can be because there were more Cr(VI) ions bound on surface of UiO-66-NH_2 with the increase of the equilibrium concentration. As the active sites on UiO-66-NH_2 were limited, the unit adsorption capacity showed a slow increase trend when the Cr(VI) content reached a certain value.

When fixed equilibrium concentration of Cr(VI) solution was used, the values of q_e increased with the increase of temperature. So the process was endothermic.

For further understanding the adsorption property, three isotherm models (shown in Table S1) were applied to fit the equilibrium data. The fitting results and parameters are shown in Fig. 5(d) and Table 2, respectively.

The Langmuir model is usually utilized to fit the single-layer adsorption process on a uniform surface [38,40]. The value of K_L was much less than 1 on both temperatures, revealing that there was a strong interaction between UiO-66-NH_2 and Cr(VI). In addition, the values of $q_{e(exp)}$ (189, 208 and 231 mg·g^{-1}) and $q_{m(theo)}$ (211, 228 and 252 mg·g^{-1}) were not far off at three temperatures, and there was high R^2 value (≥0.991) and low SSE value (≤161). Moreover, the fitted curve was highly adjacent to the experimental curve. Therefore, the Langmuir model can describe better the adsorption process of UiO-66-NH_2 toward Cr(VI).

The Koble-Corrigan model is a combination of Langmuir and Freundlich models [39]. The value of the parameter n (n=1.07, 1.00 and 0.851) was close to 1, showing that the reaction is likely to be depicted by the Langmuir model. Moreover, a large R^2 value (≥0.994) and small SSE value (≤137) were obtained from this model (as shown in Table 2), indicating the occurrence of single-layer adsorption on the uptake of Cr(VI).

The Temkin model usually describes the adsorption on an uneven surface. It was seen that the fitting curve was also close to the experimental curve with the value of R^2≥0.975 and SSE≤693. So, the model can fit the adsorption process. In short, the adsorption process of Cr(VI) on UiO-66-NH_2 was mainly a single layer adsorption on non-uniform surface [41].

2-6. Thermodynamic Study

The value of thermodynamic parameters helps to understand the feasibility of the adsorption process. In practice, this can be determined by using the Gibbs free energy (ΔG), enthalpy change (ΔH), and entropy change (ΔS).

$$K_c = \frac{C_{ad,e}}{C_e} \tag{5}$$

$$\Delta G = -RT\ln K_c \tag{6}$$

$$\Delta G = \Delta H - T\Delta S \tag{7}$$

$$\ln k = -\frac{E_a}{RT} + \ln A \tag{8}$$

where, $C_{ad,e}$ and C_e express the concentration of Cr(VI) on the adsorbent and in the solution at adsorption equilibrium and can be obtained from the first few points of the isotherm; ΔG is the Gibbs free energy (kJ·mol^{-1}); R is the gas constant (8.314 J·mol^{-1}·K^{-1}); T is the absolute temperature (K); k is the adsorption rate

constant; E_a is the apparent activation energy (kJ·mol^{-1}); A is the temperature influence factor.

According to Eq. (5)-(8), the thermodynamic parameters of the process for UiO-66-NH_2 capturing Cr(VI) are shown in Table 3. Negative ΔG shows that the process was spontaneous. It decreased from −5.04 to −7.37 kJ·mol^{-1} with the temperature increased from 293 to 313 K, indicating that the reaction was easy to happen at higher temperature [39]. The positive value of ΔH (29.0 kJ·mol^{-1}) reveals that the reaction was endothermic, while the positive value of ΔS (0.117 J·mol^{-1}·K^{-1}) tended to 0, meaning that the disorder on the surface of UiO-66-NH_2 increased slightly during the adsorption process. The value of E_a (8.21 kJ·mol^{-1}) was between 5-40 kJ·mol^{-1}, which reveals that chemical adsorption was dominant in this adsorption process. These findings are consistent with the kinetic analysis. In summary, the adsorption process was spontaneous and endothermic, and chemisorption was the main adsorption mechanism.

2-7. Exploration of Regeneration Performance

Recycling performance helps to determine the economic benefits of materials [42-44]. Therefore, it is necessary to be performed, and the results are shown in Fig. S2(b) and Fig. 6(a). It can be seen from Fig. S2(b) that the better desorption regeneration method was shown by NaOH, as well as the effect of 0.01 mol·L^{-1} NaOH was more prominent than 0.005 mol·L^{-1} NaOH. This is due to the competitive adsorption between OH^- and Cr(VI), and the process was affected by the concentration of OH^-. It was not difficult to find that NaOH can be used for the desorption of Cr(VI) from MOF [41]. Then multiple desorption regeneration studies were researched by using 0.01 mol·L^{-1} NaOH (shown in Fig. 6(a)). The results of five regenerations showed that the regeneration rate was basically maintained at 80%, although the desorption rate was basically at 35% (desorption was basically completed within 20 min). This phenomenon suggested that UiO-66-NH_2 can be reused for the removal of Cr(VI).

The existence of Cr(III) was calculated by measuring the Cr(VI) and total chromium content of the same system, 1 mol·L^{-1} HCl was used as a desorption solution to desorb Cr(III) from the material after adsorption of Cr(VI). It was found that Cr(III) only existed in the desorption solution, and there was no Cr(III) in the solution after adsorption of Cr(VI). This point indicates that a part of the adsorbed Cr(VI) was reduced to Cr(III) on the surface of UiO-66-NH_2, which was consistent with XPS analysis.

3. Simulated Water sample Research and Comparison of Adsorption Quantity

The analysis of simulated water samples is helpful for judging the feasibility of adsorbents in actual wastewater treatment. Therefore, the simulated water sample containing Cr(VI) was prepared. The results of adsorption are shown in Fig. 6(b).

It was noticed from Fig. 6(b) that the pH of the solution had a great influence on the adsorption. The removal efficiency of Cr(VI) under acidic conditions (pH=1.1) was better than at neutral pH. The removal efficiency was higher than 80% at pH=1.1 for 100 mg·L^{-1} Cr(VI) wastewater, and more than 50% at pH=6.8. These findings are consistent with the effect of pH, indicating that the

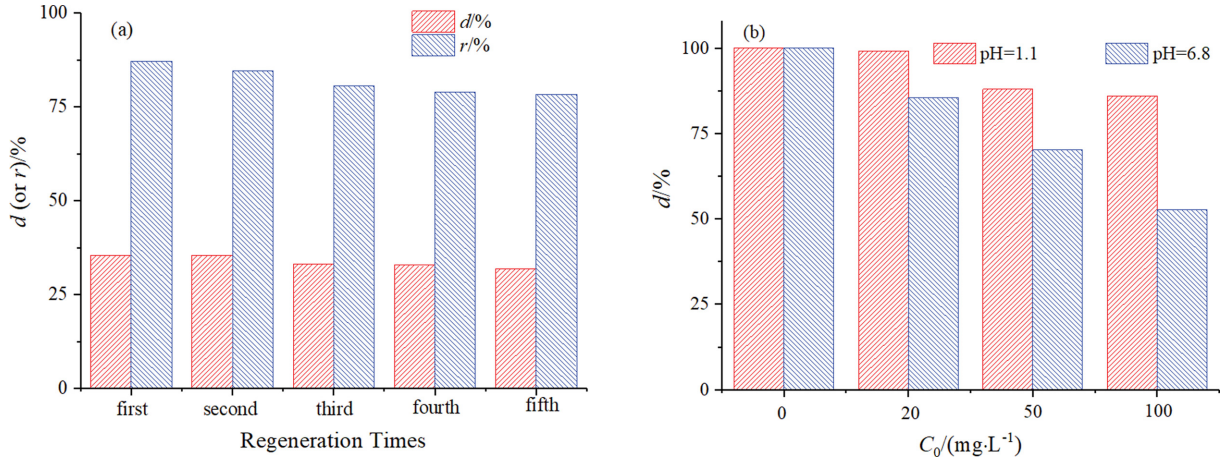

Fig. 6. (a) Research on desorption regeneration and (b) removal efficiency for simulation of wastewater research.

Table 4. Comparison of adsorbent quantity toward Cr(VI)

Adsorbent	q_e/(mg·g^{-1})	pH	Time/(h)	Ref.
PANI@NC-600	198	1.0	>6	[36]
CuNCs@HNT	79.1	5.0	>24	[1]
Zr-MOF	146	Nature pH	3	[3]
MOF-801	156	Nature pH	1	[26]
α-Fe_2O_3@C	76.9	3	2	[35]
MIL-100(Fe)	30.4	2	3	[41]
UiO-66-NH_2	252	1.1	2	This study

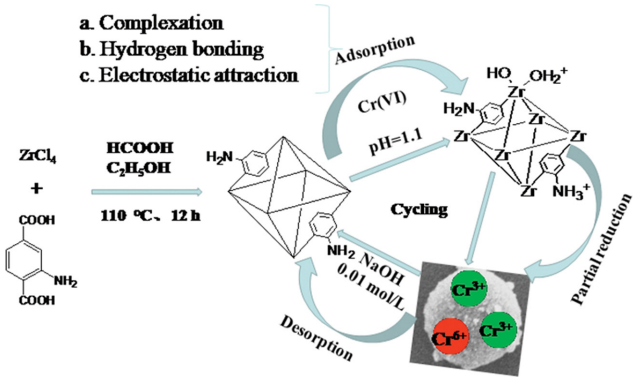

Fig. 7. Schematic illustration of adsorption mechanism.

acidic condition favored the removal of Cr(VI). This implied that UiO-66-NH_2 can be used for the removal of Cr(VI) from actual water samples.

Compared with similar adsorbents (shown in Table 4), there is highest adsorption quantity on UiO-66-NH_2 and can be a promising alternative material to remove Cr(VI) from solution with a competitive advantage.

4. Adsorption Mechanism

From FTIR and XPS analysis, the results obtained from the effects of pH and salinity were used to substantiate the adsorption mechanisms. According to the FTIR analysis, the peak of Cr-O-Cr bridge bond indicates a successful captured of Cr(VI) onto UiO-66-NH_2. The change of the peak at 1,260 cm^{-1} indicates that -NH_2/-NH_3^+ in UiO-66-NH_2 may participate in the adsorption of Cr(VI). In XPS analysis, the appearance of Cr(III) at 576.49 and 585.97 eV, showing that the adsorbed Cr(VI) was partially reduced to Cr(III). The significant changes of the N 1s peaks before and after adsorption indicate the occurrence of the hydrogen bonding/electrostatic attraction between -NH_2/-NH_3^+ and Cr(VI) during adsorption process. The content of Zr-OH in the O 1s peak was significantly reduced after adsorption. This indicates that there may be complexation between Zr-OH and Cr(VI). In addition, the effects of pH and salinity showed that there may be electrostatic attraction and complexation in the adsorption process. In summary, the adsorption process of Cr(VI) is mainly based on electrostatic attraction, hydrogen bonding, complexation and reduction. This conclusion is similar to the study reported by Wang et al. [32] for the removal of Cr(VI) using magnetic Zr-MOF. The main mechanism is shown in Fig. 7.

CONCLUSION

UiO-66-NH_2 was synthesized using one simple method and employed to adsorb and reduce Cr(VI). The results revealed that this process is mainly involved single-layer adsorption with chemical adsorption, and the electrostatic attraction, hydrogen bonding, complexation and reductive degradation are the main mechanisms governing the adsorption process. There was some tolerance for salt and property of regeneration for spent adsorbent. UiO-66-NH_2 has great potential for removing Cr(VI) from wastewater and can be considered for modifying environmentally friendly materials (such as biomass) by in-situ growth to improve the adsorption performance of cheap materials.

ACKNOWLEDGEMENTS

This work was financially supported by the Henan province basis and advancing technology research project (142300410224). The authors also acknowledge Farid Mzee Mpatani for improving the scientific language of this manuscript.

SUPPORTING INFORMATION

Additional information as noted in the text. This information is available via the Internet at http://www.springer.com/chemistry/journal/11814.

REFERENCES

1. A. K. Deb, B. Biswas, R. Naidu and M. M. Rahman, *J. Hazard. Mater.*, **421**, 126812 (2022).
2. B. Valizadeh, T. N. Nguyen, S. Kampouri, D. T. Sun, M. D. Mensi, K. Stylianou, B. Smit and W. L. Queen, *J. Mater. Chem. A*, **8**, 9629 (2020).
3. Q. Li, X. B. Cai, L. H. Chen, B. B. Guan, Z. L. Fan, W. Zhu and D. X. Xue, *Inorg. Chem.*, **60**, 8143 (2021).
4. T. C. Nguyen, X. T. Nguyen, D. M. T. Tran, Q. T. Vu, V. H. Nguyen, D. T. Nguyen, M. T. Do, T. L. Nguyen, T. N. L. Ly and H. Thai, *Bioinorg. Chem. Appl.*, **2020**, 1 (2020).
5. T. Kekes, G. Kolliopoulos and C. Tzia, *J. Environ. Chem. Eng.*, **9**, 105581 (2021).
6. J. S. Marciano, R. R. Ferreira, A. G. de Souza, R. F. S. Barbosa, A. J. de Moura Junior and D. S. Rosa, *Int. J. Biol. Macromol.*, **181**, 112 (2021).
7. S. X. Dong, Y. L. Wang, J. Y. Li, D. X. Zhang, Y. Q. Zhou and Y. Tong, *Chem. Eng. J.*, **394**, 124944 (2020).
8. M. S. Samuel, E. Selvarajan, R. Chidambaram, H. Patel and K. Brindhadevi, *Chemosphere*, **284**, 131368 (2021).
9. L. L. Fang, L. Ding, W. Ren, H. Q. Hu, Y. Huang, P. H. Shao, L. M. Yang, H. Shi, Z. Ren, K. K. Han and X. B. Luo, *J. Hazard. Mater.*, **416**, 125829 (2021).
10. X. M. Chen, W. G. Zhang, X. L. Luo, F. Zhao, Y. X. Li, R. H. Li and Z. H. Li, *Chemosphere*, **185**, 991 (2017).
11. R. Khosravi, G. Moussavi, M. T. Ghaneian, M. H. Ehrampoush, B. Barikbin, A. A. Ebrahimi and G. Sharifzadeh, *J. Mol. Liq.*, **256**, 163 (2018).
12. F. Bahador, R. Foroutan, H. Esmaeili and B. Ramavandi, *Carbohyd. Polym.*, **251**, 117085 (2021).
13. A. Hosseinkhani, B. Forouzesh Rad and M. Baghdadi, *J. Environ. Manage.*, **274**, 111153 (2020).
14. A. Zubair, H. N. Bhatti, M. A. Hanif and F. Shafqat, *Water Air Soil Pollut.*, **191**, 305 (2008).
15. A. R. Iftikhar, H. N. Bhatti, M. A. Hanif and R. Nadeem, *J. Hazard. Mater.*, **161**, 941 (2009).
16. M. Akram, H. N. Bhatti, M. Iqbal, S. Noreen and S. Sadaf, *J. Environ. Chem. Eng.*, **5**, 400 (2017).
17. S. S. Kahu, A. Shekhawat, D. Saravanan and R. M. Jugade, *Carbo-*

hyd. Polym., **146**, 264 (2016).
18. K. Y. A. Lin, Y. T. Liu and S. Y. Chen, *J. Colloid Interface Sci.*, **461**, 79 (2016).
19. S. S. Chen, Z. Y. Zang, S. S. Zhang, G. F. Ouyang and R. P. Han, *J. Environ. Chem. Eng.*, **9**, 104780 (2021).
20. L. Joseph, B. Jun, M. Jang, C. M. Park, J. C. Muñoz-Senmache, A. J. Hernández-Maldonado, A. Heyden, M. Yu and Y. Yoon, *Chem. Eng. J.*, **369**, 928 (2019).
21. M. Sarker, J. Y. Song and S. H. Jhung, *Chem. Eng. J.*, **331**, 124 (2018).
22. X. Fang, S. B. Wu, Y. H. Wu, W. Yang, Y. L. Li, J. Y. He, P. D. Hong, M. X. Nie, C. Xie, Z. J. Wu, K. S. Zhang, L. T. Kong and J. H. Liu, *Appl. Surf. Sci.*, **518**, 146226 (2020).
23. X. Y. Liu, K. O. Kirlikovali, Z. J. Chen, K. K. Ma, K. B. Idrees, R. Cao, X. Zhang, T. Islamoglu, Y. L. Liu and O. K. Farha, *Chem. Mater.*, **33**, 1444 (2021).
24. X. T. Zhang, M. Y. Liu and R. P. Han, *J. Environ. Chem. Eng.*, **9**, 106672 (2021).
25. M. Zahid, D. X. Zhang, X. Y. Xu, M. Pan, M. H. Ul Haq, A. T. Reda and W. G. Xu, *J. Hazard. Mater.*, **416**, 125835 (2021).
26. S. T. Zhuang, R. Cheng and J. L. Wang, *Chem. Eng. J.*, **359**, 354 (2019).
27. X. Y. Shi, X. D. Zhang, F. K. Bi, Z. H. Zheng, L. J. Sheng, J. C. Xu, Z. Wang and Y. Q. Yang, *J. Mol. Liq.*, **316**, 113812 (2020).
28. F. Zhao, W. X. Yang, Y. Han, X. L. Luo, W. Z. Tang, T. L. Yue and Z. H. Li, *Chem. Eng. J.*, **407**, 126744 (2021).
29. S. Lin, D. H. Kumar Reddy, J. K. Bediako, M. Song, W. Wei, J. Kim and Y. Yun, *J. Mater. Chem. A*, **5**, 13557 (2017).
30. M. M. Zhang, Q. Sun, Y. J. Wang, W. J. Shan, Z. N. Lou and Y. Xiong, *Chem. Eng. J.*, **421**, 129748 (2021).
31. Z. W. Chang, Y. J. Lee and D. J. Lee, *J. Environ. Manage.*, **247**, 263 (2019).
32. C. Wang, C. Xiong, Y. L. He, C. Yang, X. T. Li, J. Z. Zheng and S. X. Wang, *Chem. Eng. J.*, **415**, 128923 (2021).
33. X. Z. Jia, B. Zhang, C. Chen, X. Fu and Q. Huang, *Carbohyd. Polym.*, **253**, 117305 (2021).
34. M. Q. Zheng, X. D. Zhao, K. K. Wang, Y. B. She and Z. Q. Gao, *Ind. Eng. Chem. Res.*, **58**, 23330 (2019).
35. V. T. Trang, L. T. Tam, N. Van Quy, V. N. Phan, H. Van Tuan, T. Q. Huy, N. X. Dinh and A. Le, *J. Sci.-Adv. Mater. Dev.*, **5**, 392 (2020).
36. Y. X. Lai, F. Wang, Y. M. Zhang, P. Ou, P. P. Wu, Q. L. Fang, Z. Chen and S. Li, *Chem. Eng. J.*, **378**, 122069 (2019).
37. F. M. Mpatani, A. A. Aryee, A. N. Kani, Q. H. Guo, E. Dovi, L. B. Qu, Z. H. Li and R. P. Han, *Chemosphere*, **259**, 127439 (2020).
38. C. H. Ma, X. T. Zhang, K. Wen, R. Wang and R. P. Han, *Korean J. Chem. Eng.*, **38**, 135 (2021).
39. M. Y. Liu, Z. Y. Zang, S. S. Zhang, G. F. Ouyang and R. P. Han, *Int. J. Biol. Macromol.*, **182**, 1759 (2021).
40. H. N. Bhatti, Z. Mahmood, A. Kausar, S. M. Yakout, O. H. Shair and M. Iqbal, *Int. J. Biol. Macromol.*, **153**, 146 (2020).
41. M. Forghani, A. Azizi, M. J. Livani and L. A. Kafshgari, *J. Solid State Chem.*, **291**, 121636 (2020).
42. A. A. Aryee, F. M. Mpatani, Y. Y. Du, A. N. Kani, E. Dovi, R. P. Han, Z. H. Li and L. B. Qu, *Environ. Pollut.*, **268**, 115729 (2021).
43. J. L. Wang, X. Liu, M. M. Yang, H. Y. Han, S. S. Zhang, G. F. Ouyang and R. P. Han, *J. Mol. Liq.*, **338**, 116698 (2021).
44. E. Dovi, A. A. Aryee, A. N. Kani, F. M. Mpatani, J. J. Li, Z. H. Li, L. B. Qu and R. P. Han, *J. Environ. Chem. Eng.*, **9**, 106310 (2021).

Supporting Information

Removal of Cr(VI) from solution using UiO-66-NH_2 prepared in a green way

Xiaoting Zhang*, Shusheng Zhang, Gangfeng Ouyang**, and Runping Han*,†**

*College of Chemistry, Green Catalysis Center, Zhengzhou University, No 100 of Kexue Road, Zhengzhou, 450001, P. R. China
**Center for Modern Analysis and Gene Sequencing, Zhengzhou University, No 100 of Kexue Road, Zhengzhou, 450001, P. R. China
(*Received 27 September 2021 • Revised 12 November 2021 • Accepted 14 November 2021*)

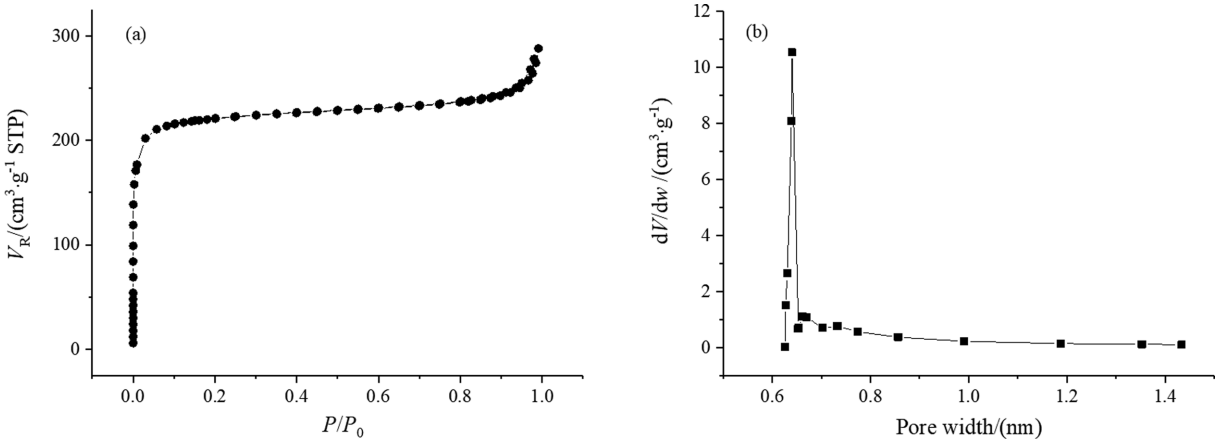

Fig. S1. (a) Isotherm curve of N_2 adsorption and (b) pore size distribution.

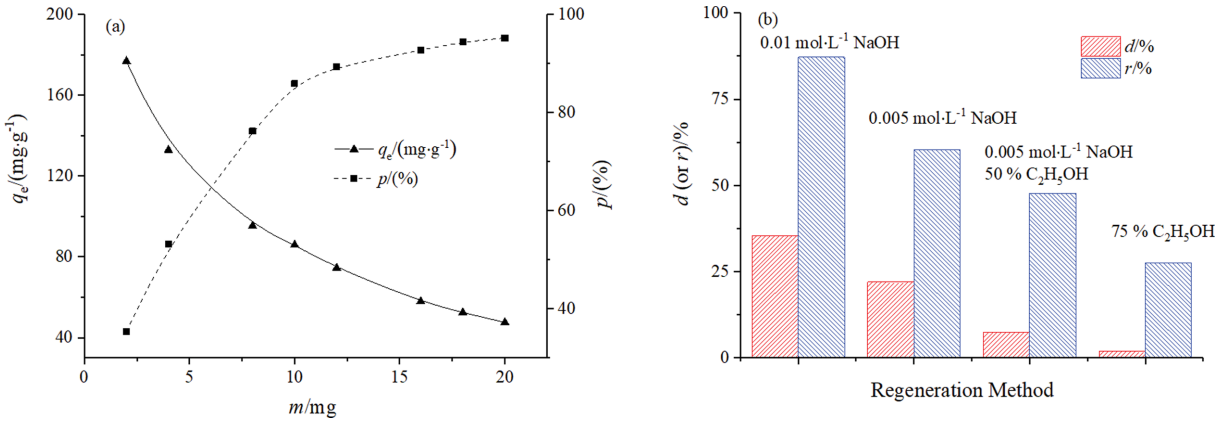

Fig. S2. (a) Effect of dosage on adsorption and (b) research on desorption regeneration method.

Table S1. Related model information

Related models	Nonlinear equation expression	Parameter description
Pseudo-first-order	$q_t = q_e(1-e^{-k_1 t})$	k_1 (min^{-1}) is the Pseudo-first-order rate constant
Pseudo-second-order	$q_t = \frac{k_2 q_e^2 t}{1+k_2 q_e t}$	k_2 ($g \cdot mg^{-1} \cdot min^{-1}$) is the Pseudo-second-order rate constant
Elovich	$q_t = A + B\ln t$	A and B are constants
Double Constant	$q_t = Ae^{K_s t}$	A is a constant, and K_s is the adsorption rate coefficient
Langmuir	$q_e = \frac{q_m K_L C_e}{1+K_L C_e}$	K_L ($L \cdot mg^{-1}$) is a constant related to binding energy; q_m ($mg \cdot g^{-1}$) is the theoretical saturated adsorption capacity of the single layer
Temkin	$q_e = A + B\ln C_e$	Both A and B are equation parameters
Koble-Corrigan	$q_e = \frac{AC_e^n}{1+BC_e^n}$	A, B and n are all equation parameters